Groundwater

Tensor Hydraulic Conductivity Estimation for Heterogeneous Aquifers under Unknown Boundary Conditions

by Jianying Jiao[1] and Ye Zhang[2]

Abstract

A physically based inverse method is developed using hybrid formulation and coordinate transform to simultaneously estimate hydraulic conductivity tensors, steady-state flow field, and boundary conditions for a confined aquifer under ambient flow or pumping condition. Unlike existing indirect inversion techniques, the physically based method does not require forward simulations to assess model-data misfits. It imposes continuity of hydraulic head and Darcy fluxes in the model domain while incorporating observations (hydraulic heads, Darcy fluxes, or well rates) at measurement locations. Given sufficient measurements, it yields a well-posed inverse system of equations that can be solved efficiently with coarse grids and nonlinear optimization. When pumping and injection are active, well rates are used as measurements and flux sampling is not needed. The method is successfully tested on synthetic aquifer problems with regular and irregular geometries, different hydrofacies and flow patterns, and increasing conductivity anisotropy ratios. All problems yield stable inverse solutions under increasing head measurement errors. For a given set of observations, inversion accuracy is strongly affected by the conductivity anisotropy ratio. Conductivity estimation is also affected by flow pattern: within a hydrofacies, when Darcy flux component is very small, the corresponding directional conductivity perpendicular to streamlines becomes less identifiable. Finally, inversion is successful even if the location of aquifer boundaries is unknown. In this case, the inversion domain is defined by the location of the measurements.

Introduction

Hydraulic conductivity (K) is a critical parameter influencing fluid flow in aquifers. Owing to subsurface heterogeneity, conductivity often exhibits large-scale anisotropy and must be represented as a tensor property in groundwater models (Zhang et al. 2006). However, because of issues related to aquifer heterogeneity, measurement scale effect, uncertain boundary conditions (BCs), and lack of efficient estimation techniques, tensor K estimation is challenging. For a confined aquifer with multiple hydrofacies, this study develops a steady-state physically based inverse method that can simultaneously estimate tensor conductivities, groundwater flow field, and the unknown aquifer BC. In the following, current inverse methods for estimating aquifer K are briefly discussed, before key features of the new method are presented.

To estimate aquifer hydraulic conductivity, existing inverse methods typically develop a forward simulation model which is calibrated against observed aquifer dynamic data such as water levels, flow rates, and solute concentrations (Zhou et al. 2014). The commonly used indirect inverse methods minimize an objective function defined as a misfit between field measurements and model simulated values. During inversion, parameters are updated iteratively using the forward model which provides the link between parameters and data. Because a forward model is needed, BCs of the model are either assumed known, or are calibrated as part of the inversion procedure. However, BCs are rarely known in real aquifers and, as demonstrated by Irsa and Zhang (2012), BC calibration can lead to nonuniqueness in the estimated parameters and flow field. This means that many combinations of parameters and BC can lead to the same objective function value, thus results of indirect inverse methods are generally nonunique (Hunt et al. 1998; Rojas et al. 2008). To address this issue, steady-state groundwater in a confined aquifer is inverted with a physically based method which simultaneously estimates hydraulic conductivity and the flow field including the unknown aquifer BC (Irsa and Zhang 2012). The method imposes fluid flow continuity by fitting a set

[1]Corresponding author: Department of Geology and Geophysics, University of Wyoming, Laramie, WY 82071; 307-766-9895; fax: 307-766-6679; jjiao1@uwyo.edu

[2]Department of Geology and Geophysics, University of Wyoming, Laramie, WY 82071.

Received October 2013, accepted March 2014.

doi: 10.1111/gwat.12202

of approximating functions of the state variables to observations at locations where they are measured, which gives rise to a set of equations that can be solved in a single step. Because no forward model is simulated, the inverse method is computationally efficient and has been successfully extended to three-dimensional flows (Zhang et al. 2014) as well as to problems with significant sources/sinks (Jiao and Zhang 2014; Zhang 2014). In these studies, aquifer conductivities were assumed locally isotropic, which however may not reflect field conditions.

Using hybrid formulation and coordinate transform, this study extends our previous works by estimating tensor conductivities for an aquifer under ambient flow or pumping condition. In ambient flow, observations needed for inversion to succeed include hydraulic heads and subsurface Darcy fluxes. When pumping is active, pumping rate can replace flux measurements. The inverse solution includes hydrofacies conductivities and head and flux approximating functions throughout the model domain. Several synthetic problems with regular and irregular aquifer geometries, different hydrofacies and flow patterns, and increasing conductivity anisotropy ratio are successfully inverted. Inversion is also successful when aquifer boundary *location* is unknown, that is, inversion domain is defined by the location of measurements, offering significant flexibility for problems where aquifer physical boundaries are either far away from the area of interest (where measurements lie) or their location is uncertain.

In the remainder of this article, the physically based inverse method is introduced, followed by results testing the method on several synthetic problems. For each problem, a forward model generates a set of "true" observations under a set of true model BCs. The observations are inverted to estimate conductivities and flow field which are compared to the forward model to assess the accuracy of inversion. Strengths and limitations of the method are discussed, and for a problem where aquifer boundary location is unknown, inverse solution is compared to one obtained with an objective function-based technique.

Theory

In this study, model coordinate is assumed aligned with conductivity principle directions, estimated K are thus diagonal tensors. Under the Dupuit-Forchheimer assumption of negligible vertical flow, the steady-state, two-dimensional (2D), incompressible flow equation for a horizontal confined aquifer is

$$\frac{\partial}{\partial x}\left(K_x b\frac{\partial h\,(x,y)}{\partial x}\right)+\frac{\partial}{\partial y}\left(K_y b\frac{\partial h\,(x,y)}{\partial y}\right)+Q\delta\,(x_0,y_0)=0 \quad \text{on } \Omega \tag{1}$$

where (x,y) is horizontal coordinate, $h(x,y)$ is hydraulic head [L], $K=\mathrm{diag}(K_x, K_y)$ [L/T], Q is pumping (positive) or injection (negative) rate per unit area at (x_0, y_0) [L/T], Ω is solution domain, b is aquifer thickness (assumed known) [L]. The horizontal Darcy flux $\boldsymbol{q}=[q_x,\ q_y]$ can be written as: $q_x=-K_x\frac{\partial h(x,y)}{\partial x}$, $q_y=-K_y\frac{\partial h(x,y)}{\partial y}$. Given hydraulic conductivities, Equation (1) can be solved in the forward mode under a set of suitable BCs.

Following our previous works, the inverse method enforces two constraints:

1. Global continuity of hydraulic head and Darcy flux throughout Ω, which can be written as:

$$\int R_h\left(\Gamma_j\right)\delta\left(p_j-\epsilon\right)d\Gamma_j=0, j=1,\ \ldots\ ,m \tag{2}$$

$$\int R_q\left(\Gamma_j\right)\delta\left(p_j-\epsilon\right)d\Gamma_j=0, j=1,\ \ldots\ ,m \tag{3}$$

where $R_h(\Gamma_j)$ and $R_q(\Gamma_j)$ are residuals of approximating functions of hydraulic head and Darcy flux at jth cell interface (Γ_j) in the inversion grid, respectively, m is the total number of cell interfaces, $\delta(p_j-\epsilon)$ is a Dirac delta weighting function which samples the residuals at a set of collocation points (p_j) on the interfaces. Both residuals can be expanded as

$$R_h\left(\Gamma_j\right)=\overline{h}^i\left(\Gamma_j\right)-\overline{h}^k\left(\Gamma_j\right) \tag{4}$$

$$R_q\left(\Gamma_j\right)=\overline{q}^i\left(\Gamma_j\right)-\overline{q}^k\left(\Gamma_j\right) \tag{5}$$

where $\overline{h}$ and $\overline{q}$ are the approximating functions, and i and k denote cells in the inversion grid adjacent to Γ_j. If Γ_j lies within a hydrofacies, $R_q(\Gamma_j)$ is written for both flux components; if Γ_j lies on a hydrofacies boundary, $R_q(\Gamma_j)$ is written for the normal flux.

2. Local conditioning of $\overline{h}$ and $\overline{q}$ to observed heads and fluxes:

$$\delta\left(p_j-\epsilon\right)\left(\overline{h}\left(p_j\right)-h^o\right)=0 \tag{6}$$

$$\delta\left(p_j-\epsilon\right)\left(\overline{q}_x\left(p_j\right)-q_x^o\right)=0 \tag{7}$$

$$\delta\left(p_j-\epsilon\right)\left(\overline{q}_y\left(p_j\right)-q_y^o\right)=0 \tag{8}$$

where p_j is a sampling point, h^o, q_x^o, and q_y^o are measured data, $\delta(p_j-\epsilon)$ is a weighting function which reflects measurement errors. When measurement errors are uncorrelated, $\delta(p_j-\epsilon)$ is proportional to the inverse of the error covariance (Hill and Tiedeman 2007). When data are error-free, $\delta(p_j-\epsilon)=1$. In this work, inversion under both error-free and random measurement errors is investigated. For problems with active pumping, Equations 7 and 8 are optional, whereas well rates (Q) are considered measurements.

To obtain the approximating functions, local analytical flow solutions are developed which are applicable to describing flow in either individual inversion grid cells or individual hydrofacies. For such a homogeneous subdomain (Ω_i), Equation 1 becomes:

$$K_x b\frac{\partial}{\partial x}\left(\frac{\partial h\,(x,y)}{\partial x}\right)+K_y b\frac{\partial}{\partial y}\left(\frac{\partial h\,(x,y)}{\partial y}\right)+Q\delta\,(x_0,y_0)=0 \quad \text{on } \Omega i \tag{9}$$

Equation 9 is linear for which a local analytical flow solution can be found:

$$\overline{h}(x,y) = a_1 + a_2 x\left(\frac{K_y}{K_x}\right)^{0.25} + a_3 y\left(\frac{K_x}{K_y}\right)^{0.25} + a_4 xy + a_5 x^2\left(\frac{K_y}{K_x}\right)^{0.5} - a_5 y^2\left(\frac{K_x}{K_y}\right)^{0.5} + \frac{Q}{4\pi b\sqrt{K_x K_y}} \times \ln\left((x-x_0)^2\left(\frac{K_y}{K_x}\right)^{0.5} + (y-y_0)^2\left(\frac{K_x}{K_y}\right)^{0.5}\right) \quad \text{on } \Omega i \tag{10}$$

where a_1, a_2, a_3, a_4, and a_5 are coefficients of the subdomain to be determined by inversion, K_x and K_y are unknown component conductivities of Ω_i, Q is a (known) well rate at $(x_0, y_0) \in \Omega_i$. Equation 10 is obtained by transforming the original model coordinate where K is diagonal to a new coordinate where it is scalar: (1) in the new coordinate, analytical solution is developed for Equation 9 using superposition; (2) transform the analytical solution back to the original coordinate (Chin 2006). For example, the last term of Equation 10 is based on transforming the Thiem solution for an infinite, homogeneous, isotropic confined aquifer with a fully penetrating well of zero radius; the first six terms describe a superimposed background flow (i.e., a solution of the Laplace equation) that arises owing to regional BC or local hydrofacies variations. A single well is represented in Equation 10. If more than one well exist, Equation 10 will be developed for each well. Based on Equation 10, Darcy flux in Ωi can be written as

$$\overline{q}_x(x,y) = -K_x\left(a_2\left(\frac{K_y}{K_x}\right)^{0.25} + a_4 y + 2a_5 x\left(\frac{K_y}{K_x}\right)^{0.5} + \frac{Q\left((x-x_0)\left(\frac{K_y}{K_x}\right)^{0.5}\right)}{2\pi b\sqrt{K_x K_y}\left((x-x_0)^2\left(\frac{K_y}{K_x}\right)^{0.5} + (y-y_0)^2\left(\frac{K_x}{K_y}\right)^{0.5}\right)}\right) \quad \text{on } \Omega i \tag{11}$$

$$\overline{q}_y(x,y) = -K_y\left(a_3\left(\frac{K_x}{K_y}\right)^{0.25} + a_4 x - 2a_5 y\left(\frac{K_x}{K_y}\right)^{0.5} + \frac{Q\left((y-y_0)\left(\frac{K_x}{K_y}\right)^{0.5}\right)}{2\pi b\sqrt{K_x K_y}\left((x-x_0)^2\left(\frac{K_y}{K_x}\right)^{0.5} + (y-y_0)^2\left(\frac{K_x}{K_y}\right)^{0.5}\right)}\right) \quad \text{on } \Omega i \tag{12}$$

For a given inversion grid, Equations 10 to 12 are discretized with a hydrofacies-based K parameterization which is in effect a form of regularization (Moore and Doherty 2006). No other prior information is assumed. In the inversion grid, grid cells honor hydrofacies boundaries but generally coarsen away from these boundaries. Because analytical solutions are created to represent pumping, local grid refinement (LGR) at wells is not needed. Furthermore, because analytical solutions are populated in a piecewise manner, the inversion grid can be highly flexible, for example, voxel connection is not necessary. Following discretization, Equations 2 and 3 are written at all inversion grid cell interfaces and Equations 6 to 8 at the measurement locations. The equations are nonlinear, and depending on measurement support, can be underdetermined, exact, or overdetermined. Here, sufficient observations are provided to inversion, the equation systems are overdetermined which can lead to stable solutions. The equations are minimized with two gradient-based optimization techniques, that is, Levenberg-Marquardt and Trust-Region-Reflective (Moré 1977; Coleman and Li 1996). Both algorithms are implemented in Matlab's *lsqnonlin*, which solves a least-squares problem (The Mathworks 2012):

$$\min_x \| f(\boldsymbol{x}) \|_2^2 = \min_x \left(f_1(\boldsymbol{x})^2 + f_2(\boldsymbol{x})^2 + \cdots + f_n(\boldsymbol{x})^2\right) \tag{13}$$

where $\boldsymbol{x}$ is the inverse solution: $\boldsymbol{x}^T = [a_1^l, a_2^l, a_3^l, a_4^l, a_5^l, K^m]$, $l = 1, \ldots, M$ (number of inversion cells), $m = 1, \ldots, R$ (number of hydrofacies), and $f_1(\boldsymbol{x})$, $f_2(\boldsymbol{x})$, $\ldots$, $f_n(\boldsymbol{x})$ are the equations assembled according to Equations 2 to 8. Constraints can also be placed on $\boldsymbol{x}$, for example, enforcing positive conductivities. From the solution, K are estimated and $\overline{h}$ and $\overline{q}$ (one set for each inversion cell) recovered. BC (either head or flux) can be obtained by sampling the appropriate $\overline{h}$ and $\overline{q}$.

As discussed in Hill and Tiedeman (2007), unique conductivity estimation requires *both* hydraulic heads and measurements related to head gradient, that is, fluxes or flow rates. This study first investigates ambient flow for which subsurface Darcy fluxes are sampled, and $\overline{h}$ and $\overline{q}$ are obtained by setting $Q = 0$ in Equations 10 to 12. Next, a problem with active pumping and injection is inverted for which Equations 10 to 12 are implemented in a hybrid formulation: Q is specified to a "well cell" and is zero outside the well cell. The size of the well cell must be carefully adjusted so that it is sufficiently large to accommodate a number of observed heads (≥ 2) which help condition the local solution inside the well cell. This size is also influenced by proximity to boundaries—if BC significantly impacts pumping, the well cell dimensions

must be reduced. Reversely, if BC influence on pumping is insignificant, the well cell can encompass a greater area. Overall, the local solution inside the well cell must not be strongly influenced by BC. Instead, BC influence is reflected in the solutions of grid cells between the well cell and the model boundary. This hybrid formulation leads to significant computational savings, as the number of unknown coefficients is kept low.

Results

To use synthetic aquifers to test the inverse method, forward (true) models are first simulated to provide the inversion with observations. These models are simulated with MODFLOW2000 (Harbaugh et al. 2000), with a horizontal base set as the head datum. When pumping and injection are active, grid cells near wells are increasingly refined until drawdowns no longer change with grid refinement. The inverse method is tested next by comparing the estimated K and the recovered flow fields to those of the forward models. Five problems with regular aquifer shapes are investigated, followed by three with complex geometries—in the last problem, the aquifer boundary location is unknown and the inversion grid is defined by the measurement location.

For selected problems, stability tests are conducted to access inversion under increasing measurement errors. Because finite difference model (FDM) is used for the forward simulation, measurements sampled from this model are considered error-free, that is, "true" heads or "true" fluxes. To impose errors, for example, the true heads are corrupted by random noises: $h^m = h^{\mathrm{FDM}} \pm \Delta h$, where h^m is the measured head provided to inversion, h^{FDM} is the true head, and Δh is the measurement error. The highest Δh is $\pm 1\%$ of the total head variation of the forward model, with an absolute error up to ± 0.2 feet. This is reasonable considering that modern measurement techniques can determine water level with a precision less than 1 cm (Post and von Asmuth 2013). In the following, units of the relevant quantities are: K in ft/d (1 ft/d = 0.305 m/d), q in ft/d (1 ft/d = 0.305 m/d), h in feet (1 ft = 0.305 m), flow rate in ft^3/d (1 $ft^3/d = 0.028\ m^3/d$). Alternatively, a consistent set of units can be assumed (Neuman et al. 2007).

Regular Domain

Five problems (cases 1 to 5), of regular shapes (Figure 1), are first inverted. Forward models (or FDM) of these cases are of the same dimensions ($L_x = 1000$ feet and $L_y = 1000$ feet), discretization (50×50 grid), and BCs, with true K value listed in Tables 1 and 2. Cases 1, 2, and 3 pertain to a homogeneous aquifer with increasing conductivity anisotropy ratio (K_y/K_x) (Table 1), for which eight heads were sampled from the FDM in a quasi-regular pattern (not shown). In inversion, a 2×2 uniform grid is used. In cases 1 and 2, two Darcy flux vectors ($\boldsymbol{q}$) were sampled from the FDM, at location corresponding to the centers of the two left-hand-side inversion cells. In case 3, seven $\boldsymbol{q}$ were randomly sampled, although each inversion cell has at least one $\boldsymbol{q}$ measurement.

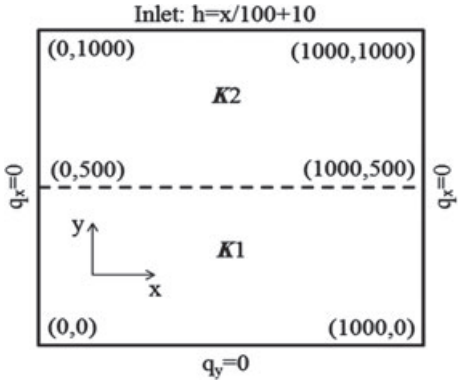

Figure 1. Forward true model with true BC. In cases 1 to 3, a single K tensor is estimated. Dashed line indicates an interface for cases 4 and 5, where 2 K zones (labeled "K1," "K2") exist. The length unit is in ft.

Table 1
Estimated K (ft/d) for Cases 1 to 3 under Increasing Measurement Errors

	Conductivity		Measurements	Grid
FDM (case 1)	$K_x = 1$	$K_y = 5$		50×50
Head error = 0%	1	4.91	8 heads + 2 $\boldsymbol{q}$	2×2[1]
Head error = ±0.5% (±0.05 feet)	0.85	4.88	8 heads + 2 $\boldsymbol{q}$	2×2
Head error = ±1% (±0.1 feet)	0.37	4.3	8 heads + 2 $\boldsymbol{q}$	2×2
FDM (case 2)	$K_x = 1$	$K_y = 10$		50×50
Head error = 0%	0.91	10.63	8 heads + 2 $\boldsymbol{q}$	2×2
Head error = ±0.5% (±0.05 feet)	0.037	10.42	8 heads + 2 $\boldsymbol{q}$	2×2
Head error = ±1% (±0.1 feet)	0.025	10.99	8 heads + 2 $\boldsymbol{q}$	2×2
FDM (case 3)	$K_x = 1$	$K_y = 100$		50×50
Head error = 0%	0.998	100.7	8 heads + 7 $\boldsymbol{q}$	2×2
Head error = ±0.1% (±0.01 feet)	1.32	94.64	8 heads + 7 $\boldsymbol{q}$	2×2
Head error = ±0.5% (±0.05 feet)	1.13	15.37	8 heads + 7 $\boldsymbol{q}$	2×2

[1] Inversion is carried out with a uniform grid: $\Delta x = \Delta y = 500$ feet.

In case 1, when error-free heads are provided to inversion, the estimated K are close to their true values. The absolute estimation errors ($|K_x^{\mathrm{true}} - K_x^{\mathrm{est}}|$; $|K_y^{\mathrm{true}} - K_y^{\mathrm{est}}|$) range from 0 to 1.8% of the true K. Compared to the FDM, the inverted streamlines and head contours are reasonably accurate, although local deviations exist (Figure 2). When the same heads, imposed with ±0.5% error, are used, the estimated K are reasonably accurate, with the absolute relative errors ($|K_x^{\mathrm{true}} - K_x^{\mathrm{est}}|/K_x^{\mathrm{true}} \times 100\%$; $|K_y^{\mathrm{true}} - K_y^{\mathrm{est}}|/K_y^{\mathrm{true}} \times 100\%$) ranging from 2.4 to 15%. When error is further increased to ±1.0%, the estimated K become less accurate—the absolute relative errors range from 14% to 63%. Despite the higher K estimation errors, the inversely recovered flow solutions are stable.

In case 2, anisotropy ratio (K_y/K_x) of the FDM is increased to 10. The same measurement and inversion

Table 2
Estimated K (ft/d) for Cases 4 and 5 under Increasing Measurement Errors

	Conductivity					
	$K1$		$K2$		Measurements	Grid
FDM (case 4)	$K1_x = 1$	$K1_y = 5$	$K2_x = 10$	$K2_y = 50$	16 heads + 4 $\boldsymbol{q}$	50×50
Head error = 0%	0.98	5.15	11.3	51.6	—	4×4
Head error = ±0.1% (±0.01 feet)	0.91	3.68	11.6	51.6	—	4×4
Head error = ±0.5% (±0.05 feet)	0.65	1.36	12.1	52	—	4×4
FDM (case 5)	$K1_x = 1$	$K1_y = 10$	$K2_x = 10$	$K2_y = 100$	16 heads + 8 $\boldsymbol{q}$	50×50
Head error = 0%	1.16	11.5	10.2	98.6	—	4×4
Head error = ±0.1% (±0.01 feet)	1.15	11.3	10.2	98.9	—	4×4
Head error = ±0.5% (±0.05 feet)	1.06	10.8	10.2	100.4	—	4×4

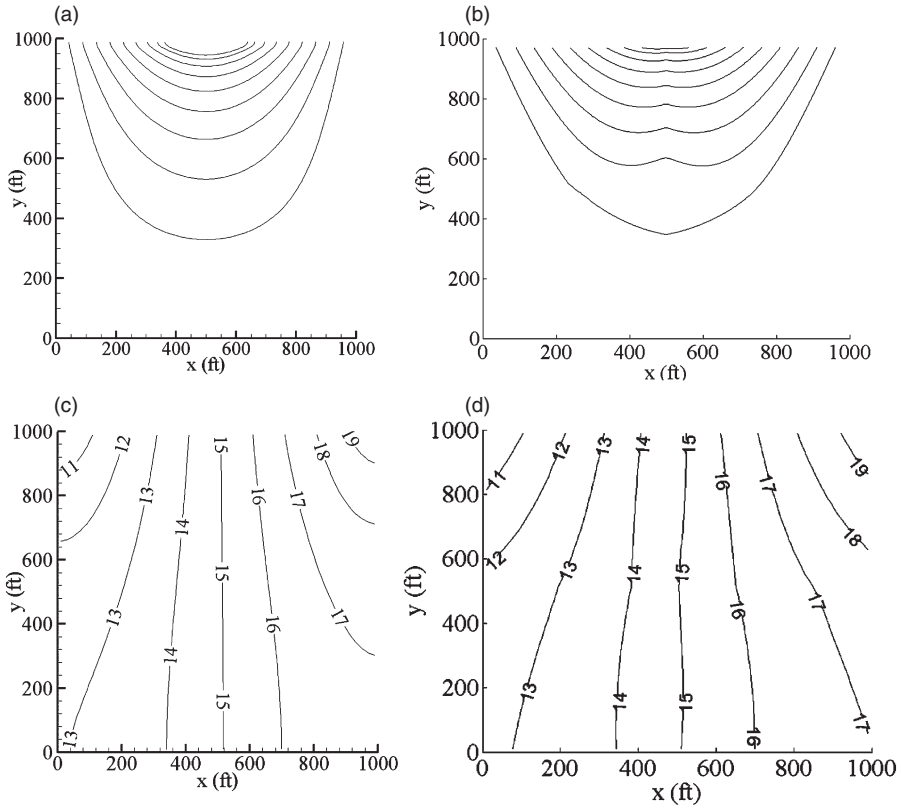

Figure 2. Case 1 results based on error-free observations. Streamlines of the FDM (a) and the inverted model (b). Hydraulic head distribution of the FDM (c) and the inverted model (d).

grid of case 1 are used. When heads are error-free, K absolute relative errors range from 6.3% to 9%, higher than those of case 1. When error is increased to ±0.5% and ±1%, respectively, higher K estimation errors are also observed for case 2. For a fixed quantity and quality of the observations, inversion accuracy suffers with increasing K_y/K_x.

In case 3, K_y/K_x of the FDM is increased to 100. Compared to cases 1 and 2, five extra $\boldsymbol{q}$ are sampled. When error-free observed heads are used, K absolute relative errors now range from 0.2% to 0.7%, lower than those of cases 1 and 2. Clearly, despite the higher anisotropy, the additional flux measurements can improve K estimation. When heads contain ±0.5% error, the absolute relative errors of K range from 13% to 85%, while the corresponding errors are 2.4% to 15% (case 1) and 4.2% to 96% (case 2). The recovered head distribution compares well to that of the FDM, but degrades under increasing measurement errors (Figure 3).

Two more problems (cases 4 and 5), each with two hydrofacies (Figure 1), are inverted with a 4×4 grid. For case 4, 16 heads were sampled from the FDM at location corresponding to the center of each inversion cell. Four $\boldsymbol{q}$ were randomly sampled (each hydrofacies has two fluxes). For case 5, the same heads were sampled with eight randomly sampled $\boldsymbol{q}$ (each hydrofacies has four fluxes). Case 5 has higher K_y/K_x than case 4. When observed heads are error-free, absolute K estimation errors are relatively

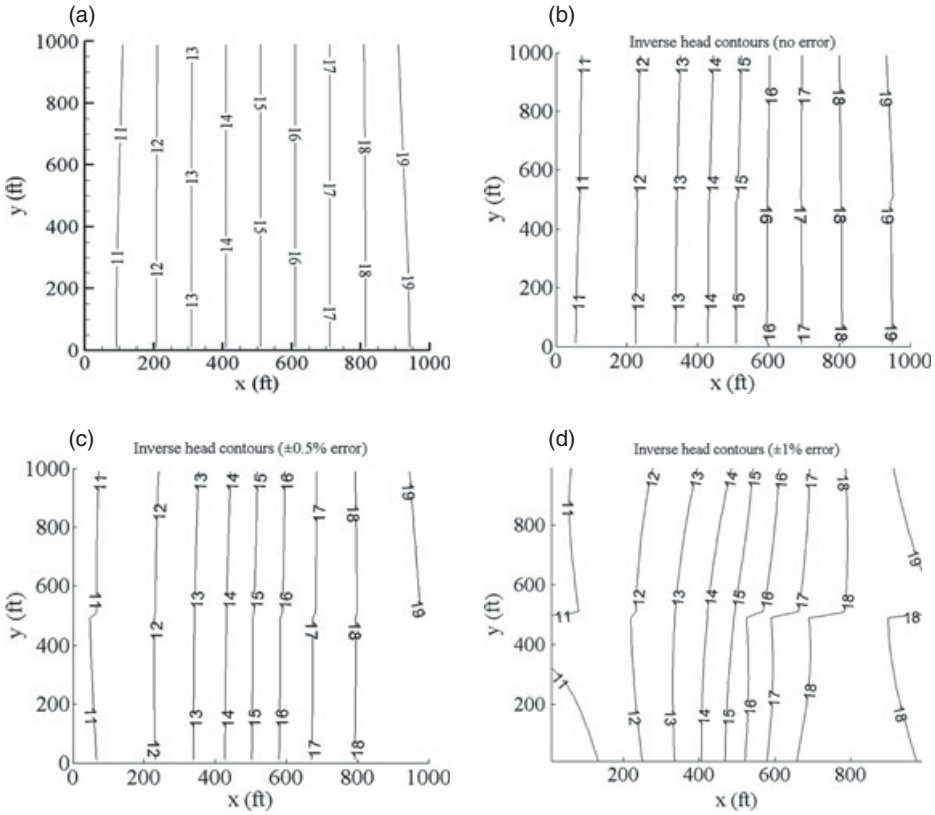

Figure 3. Hydraulic head distribution for case 3: the FDM (a) and the inverted models given error-free (b), ±0.5% (c), and ±1% (d) head measurement errors.

small (1.4% to 16%) for both cases (Table 2). Despite the extra flux measurements, estimation errors of case 5 are higher than those of case 4. Higher anisotropy ratio again poses a challenge for inversion. For case 4, when head errors increase, K errors increase, as expected. For case 5, however, K errors decrease slightly with increasing head errors. Different error sources may have compensated in contributing to the overall estimation accuracy. For both cases, when head errors are small, the recovered streamlines and head contours are quite excellent (not shown).

Irregular Domain

Ambient flow is investigated first for which the FDM grid, hydrofacies distribution, and associated true BCs are shown (Figure 4a). Both aquifer boundaries and hydrofacies pattern are known to inversion for which a coarse grid is developed (Figure 4b). At cells 10, 11, 16, and 17, we can see that voxel connection is not necessary. Measurement locations are also shown (Figure 4b): 62 heads and 20 $\boldsymbol{q}$ were sampled. Head solution of the FDM is shown in Figure 4c, compared to the recovered head under ±0.2% head measurement error (Figure 4d). Inversion yields accurate head recovery and estimated K (Table 3).

For the same aquifer geometry, a pair of pumping and injection wells, operating at a constant rate of 300 ft^3/d, are added (Figure 5a). BCs of the FDM were adjusted (Figure 5a), while the same 62 observed heads were sampled (fluxes were not sampled). Both well rates are known to inversion. The same 31-cell inversion grid (Figure 4b) is used: the well cells (pumping in cell 11, injection in cell 21) are large without LGR. Head recovery (Figure 5c and 5d) and K estimation (Table 3) are accurate when measurement errors are small.

Finally, the ambient flow problem is repeated but the location of true model boundaries is not known to inversion. From the FDM, 18 (error-free) heads and 4 q are randomly sampled within a subdomain of the full model (Figure 6a; 'a-b-c-d-a'). Given these measurements, a 3×2 inversion grid spanning the subdomain is generated (not shown). The recovered "boundary" heads along 'a-b-c-d-a' are very close to the true heads sampled from the FDM (Figure 6b). The estimated K are also close to their true values (Table 4). Had the inversion been carried out over the entire FDM, however, the estimation errors would be higher because approximating functions in the regions between subdomain and full domain boundaries (where measurements do not exist) would be extrapolations. Clearly, new inversion can be used for a problem where aquifer physical boundaries are either far away from the area of interest (where measurements lie) or are poorly known, which is typical in field situations. To apply this method, the inversion domain should be defined by the measurement location and it is not necessary or even desirable to seek "physical" boundaries where measurements do not exist.

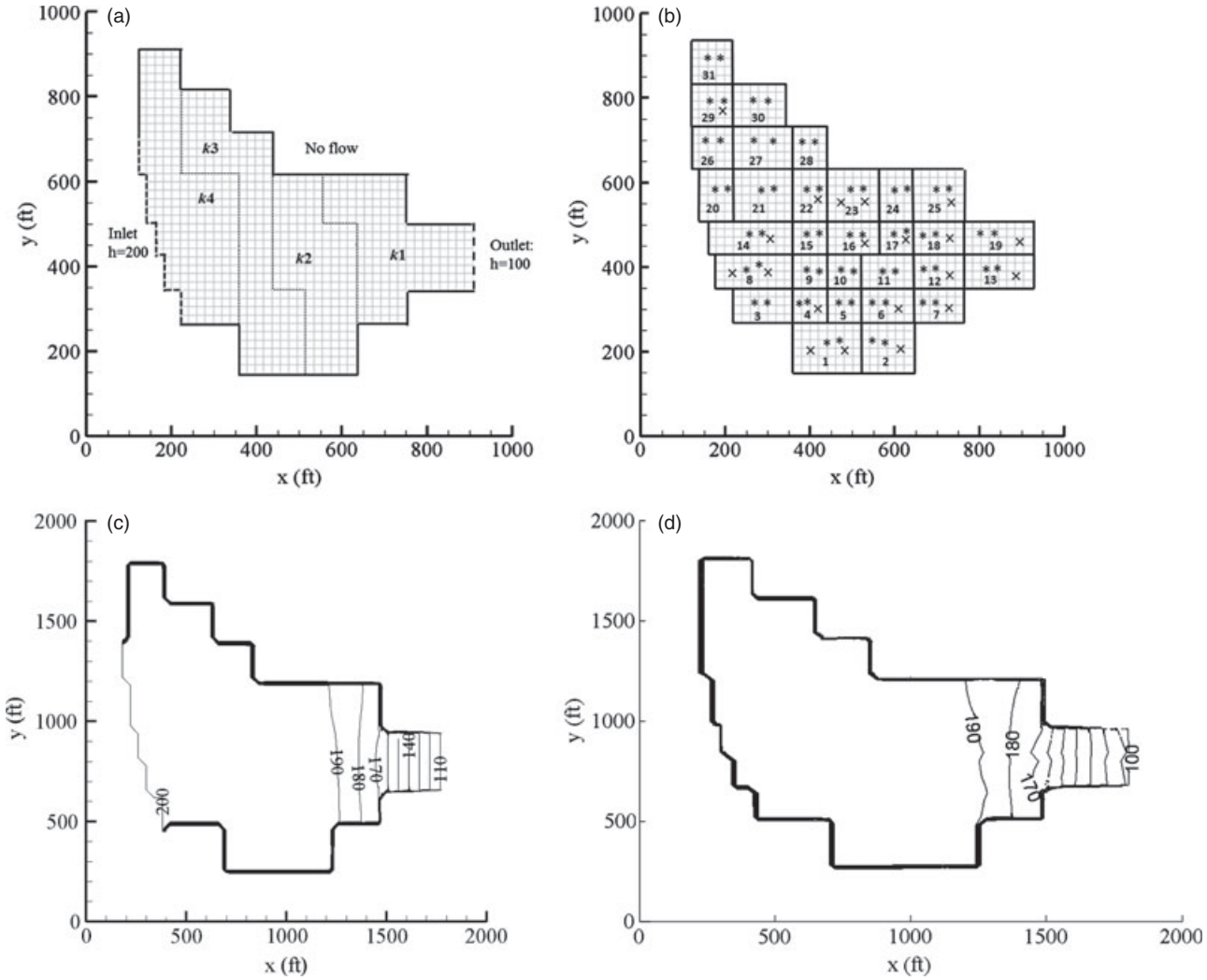

Figure 4. (a) FDM with four hydrofacies and specified aquifer BC. (b) Inversion grid (cell ID is shown) and measurement location (* denote 62 heads; × denote 20 flux vectors). (c) FDM head contours; (d) recovered head contours when observed heads contain ±0.2% error. The same contour levels of (c) are used.

Table 3
Estimated K (ft/d) for the Irregular Problems under Increasing Measurement Errors

		Conductivities							
		$K1$		$K2$		$K3$		$K4$	
FDM		$K1_x = 1$	$K1_y = 5$	$K2_x = 5$	$K2_y = 25$	$K3_x = 10$	$K3_y = 50$	$K4_x = 20$	$K4_y = 100$
Ambient flow	Head error = 0%	0.92	3.2	4.6	29.2	9.6	51.4	16.6	90.2
	Head error = ±0.2% (±0.2 feet)	0.9	3.0	4.8	26.6	9.6	51.4	15.7	72.7
	Head and flux errors = ±0.2%	0.9	3.0	4.8	26.6	9.6	51.4	15.7	72.8
Pumping and injection	Head error = 0%	1.2	3.0	5.4	29.3	12.1	56.5	21.0	99.1
	Head error = ±0.2% (±0.08 feet)	1.1	4.1	5.3	30.1	11.5	53.7	20.9	94.8
	Head and pumping rate errors = ±0.2%	1.1	4.1	5.3	30.1	11.5	53.9	21.0	95.0

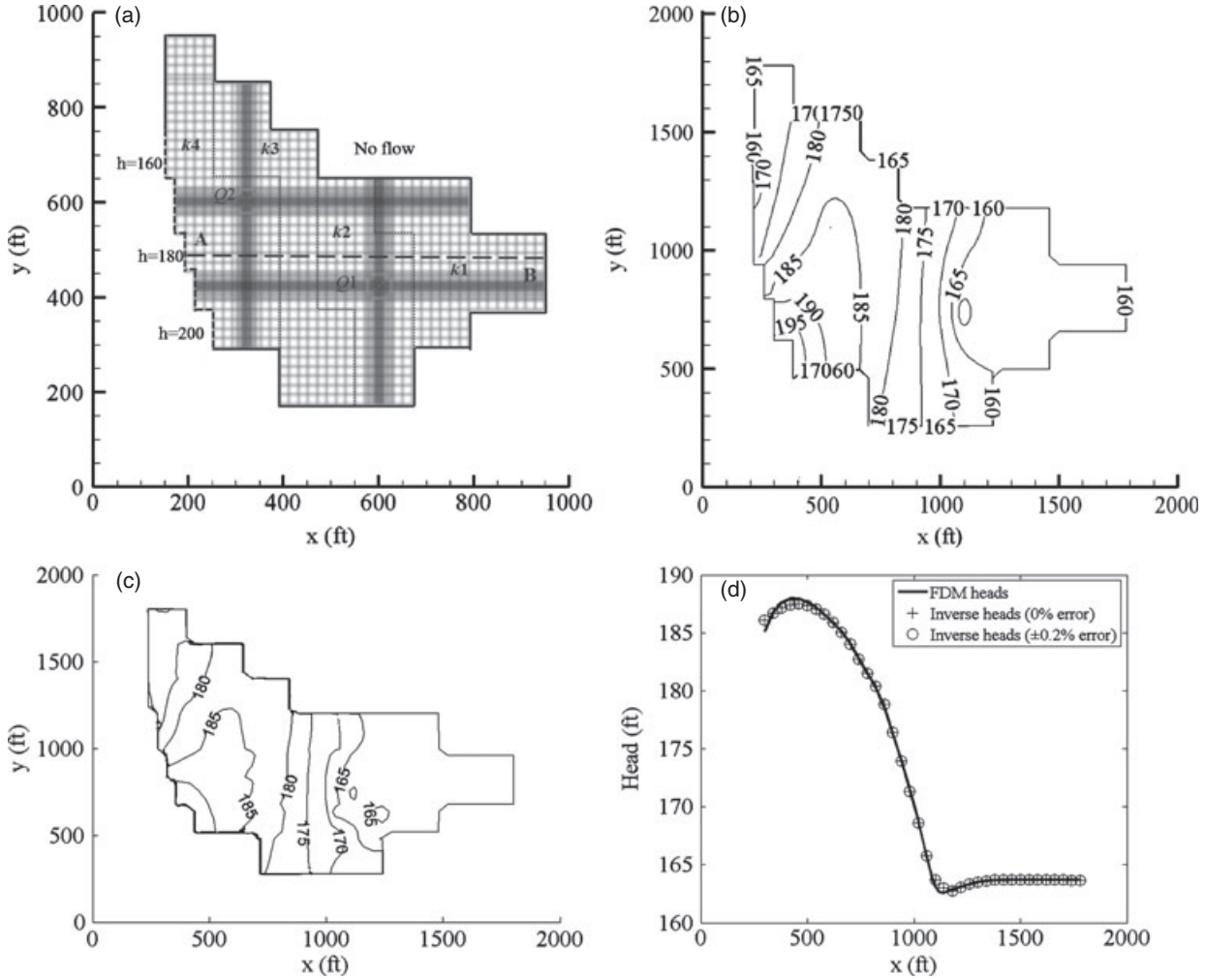

Figure 5. (a) FDM with four hydrofacies and specified BC. Pumping and injection are simulated with LGR at each well: $Q1 = -300\,ft^3/d$ (pumping) at (1100, 740) and $Q2 = 300\,ft^3/d$ (injection) at (540, 1100). Location of a profile, AB, is shown. (b) FDM head contours; (c) recovered head contours with 31 cells (Figure 4b) when head error is ±0.2%. The same contour levels of (b) are used. (d) Head profiles along AB by the FDM and by inversion under increasing head measurement errors.

Discussion

Inverse solutions for different flow fields, BCs, and conductivity anisotropy ratios reveal that, in general, parameter estimation errors arise mostly from inadequate quantity and quality of the observation data, while inversion grid discretization has secondary effect. For several synthetic problems, adding high-quality measurements can improve estimation accuracy. The selection of data location, however, is an issue not treated here. Because adding insensitive observations will not generally lead to more accurate results (Hill and Tiedeman 2007), data location optimization will be addressed in the future by combining inversion with a parameter sensitivity analysis. Moreover, if the inversion domain is defined by the location of measurements, accuracy of inversion (i.e., both conductivities and recovered flow field) can be very good, because errors due to extrapolating the approximating functions to regions *beyond* the observations are limited. For problems where the inversion domain extends to physical boundaries (e.g., river, no-flow outcrops), large regions may exist in the model without observations where extrapolation errors are expected to be high. To apply the new inversion, it is recommended to limit the solution domain to the measurement location. In addition, for problems with pumping and injection, inverse solutions can be obtained successfully with coarse grids, because well solutions are directly implemented in the inverse formulation. For these problems, subsurface flux measurements are not needed. Finally, because the inverse method does not evaluate any forward model-data misfit, it is computationally efficient. In comparison, most indirect inverse methods are computationally intensive, as they require repeated forward simulations in order to minimize the objective function, which also requires BC knowledge. If BCs are unknown, indirect methods may resort to their calibration, although this approach will likely be inefficient, as Irsa and Zhang (2012) has proven that BC calibration can lead to nonunique estimates of the parameters and flow fields.

Nonunique parameter estimation due to uncertain BC is illustrated by calibrating the previous subdomain

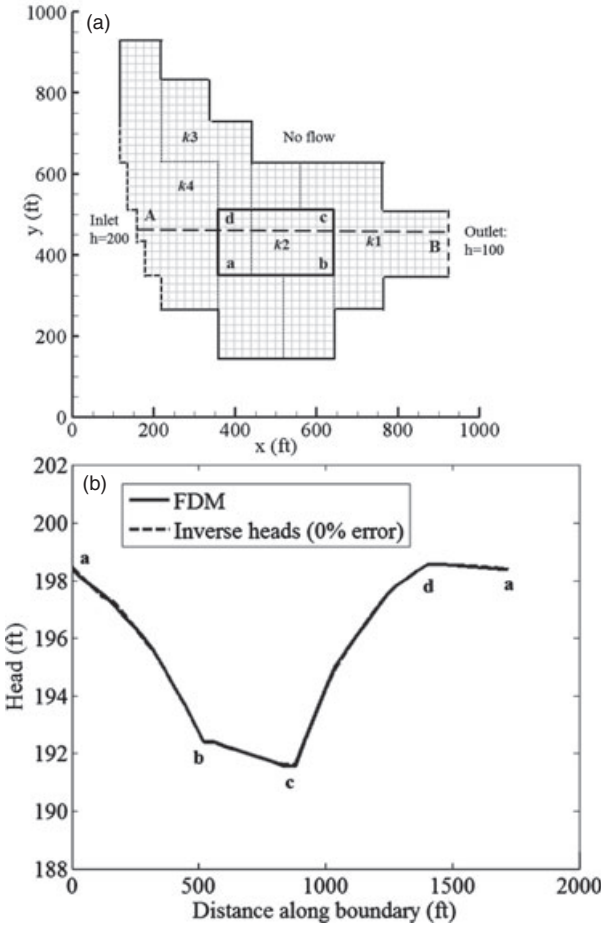

Figure 6. Subdomain inversion. (a) Subdomain (a-b-c-d-a) inside the full FDM of the ambient flow problem. (b) Recovered heads along a-b-c-d-a, compared to those sampled from the FDM.

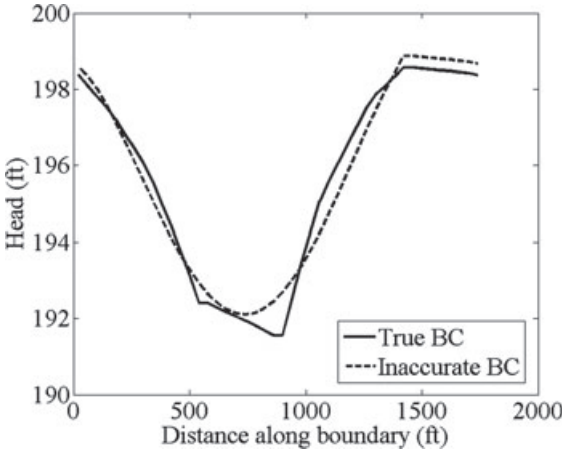

Figure 7. Hydraulic heads sampled from the FDM along the subdomain boundaries ("True BC"). These BCs are assigned to a forward subdomain model for PEST calibration. Based on the True BC, a perturbed set of BC ("Inaccurate BC") is also given to PEST.

problem (Figure 6) with PEST (Doherty 2005). A forward model, which is needed for PEST calibration, is extracted from the full FDM at the subdomain location with a 14×8 sub-grid (Figure 6a). The *same* error-free observations (18 heads and 4 $\boldsymbol{q}$) were sampled. For initial parameter guess, true K are used as the starting parameters. To run the forward model, two different BCs are postulated along the subdomain boundaries (Figure 7), leading to different results (Table 4). When the forward model is given the true BC sampled from the FDM, K estimated by PEST are close to the true values. However, when a set of perturbed BC (Figure 7) are given to PEST, the estimated K become inaccurate even though their true values are used as the initial guess. Given similar convergence criteria, the final weighted residuals are -3.68×10^{-4} (true BC) and -1.78×10^{-2} (inaccurate BC). Sensitivities computed by PEST for each parameters are: K_{2x}: 4.7×10^{-3}; K_{3x}: 4.7×10^{-3}; K_{2y}: 9.0×10^{-3}; K_{3y}: 2.1×10^{-3} (true BC), and K_{2x}: 5.4×10^{-4}; K_{3x}: 5.4×10^{-4}; K_{2y}: 3.9×10^{-4}; K_{3y}: 6.5×10^{-2} (inaccurate BC). When inaccurate BC are assigned to the forward model, both the residual and relative sensitivity suggest difficulty in estimating K_{2x}, K_{3x}, and K_{2y}, and in further lowering of the objective function. In this case, by forcing the forward model to "fit" 40 boundary heads (all of which contain errors), these errors overwhelm the *accurate* 18 heads and 4 $\boldsymbol{q}$ provided to PEST. In comparison, parameters and BCs are simultaneously estimated by the new inversion, and unlike PEST, BC knowledge is not needed. The new method yields a "unique" solution, while PEST results are sensitive to the BC assumption.

In ambient flow, when groundwater becomes stagnant in local areas (i.e., $q_x \sim 0$, $q_y \sim 0$), it becomes difficult to estimate the local conductivity. This is because both

Table 4

Estimated K (ft/d) of the Subdomain with New Inversion and with PEST Given the Same Error-Free Observations

		Conductivities				
	Grid	$K2$		$K3$		BC
FDM (subdomain)	14×8	$K2_x = 5$	$K2_y = 25$	$K3_x = 10$	$K3_x = 50$	True subdomain BC sampled from FDM
New method	3×2	4.4	25.0	8.7	50.3	Estimated by inversion
PEST	14×8	4.4	22.4	10.9	62.1	True BC assigned
PEST	14×8	0.006	6.2×10^{-8}	4.8×10^{3}	9.6×10^{3}	Inaccurate BC assigned

Note: For PEST, two sets of assumed subdomain BC are used.

head gradients and Darcy fluxes are small in these areas, thus the estimated conductivity becomes less accurate. Similarly, when flow is uniform and is parallel to a principal conductivity, it becomes difficult to find the conductivity component in the direction perpendicular to flow. For example, in a problem where dominant flow is along the y axis, q_x component of the fluxes is generally small, as is $\partial h/\partial x$. Using Darcy's law, K_x is obtained by dividing a small q_x (with numerical error) by a small $\partial h/\partial x$ (also contains error). Owing to floating point limitations, K_x cannot be accurately computed although higher precision arithmetic may improve this outcome. In comparison, when radial flow exists due to pumping, $\boldsymbol{q}$ near wells are nonnegligible in all directions. This information is integrated into the well rate; therefore, even if a similar number of heads are sampled compared to ambient flow, K_x and K_y estimation near the well location is more accurate. As distance from the well increases, flow field may become more uniform or become parallel to one coordinate. At such locations away from wells, local component conductivity in the direction perpendicular to flow again becomes less identifiable.

To apply the new method to *ambient* flow problems, subsurface Darcy fluxes are needed. Indirect techniques exist for measuring fluxes, including tracer experiments (Davis et al. 1980; Ptak et al. 2004), point dilution methods (Grisak et al. 1977, Novakowski et al. 2006), and borehole flowmeters (Molz et al. 1994; Gellasch et al. 2013). With point dilution, it is possible to estimate horizontal fluxes surrounding a borehole (Pitrak et al. 2007). With flowmeters, vertical fluxes can be determined. Instruments have also been developed to directly measure groundwater velocity near wellbores (Labaky et al. 2009). With the Point Velocity Probe, velocity magnitude and direction can both be measured from which flux vectors can be determined if porosity is known. Methods have also been developed to interrogate horizontal and vertical permeabilities over a greater rock volume than the typical logging scale (Domzalski et al. 2003). Fluxes averaged over a greater aquifer volume can thus be obtained. Therefore, groundwater flux measurement is possible if appropriate tests are conducted or if new measurement technology is developed. Moreover, if fluxes are not available, *subsurface* flow rate measurement can be used, which gives an average flux depending on at what scale the flow rate is measured. In Irsa and Zhang (2012), flow rates are used for inversion without sampling fluxes. Zhang et al. (2014) solved 3D inversion alternatively with flow rate and flux measurements. In inverting hydrofacies conductivities, subsurface fluxes and flow rates are found to possess similar "information content" (Zhang 2014). Compared to large-scale flow rates, point-scale fluxes may have the potential to resolve local conductivities at greater accuracy. Finally, like hydraulic heads, fluxes and pumping rates can also be subject to measurement errors. Additional inversions are carried out for the irregular domain problems where random errors are imposed onto *both* heads and fluxes (ambient flow) or both heads and pumping rates (pumping condition). The estimated K (Table 3) and flow fields (not shown) are not appreciably worsened compared to those when only the observed heads were subject to errors. In this case, random errors of the observed heads and observed fluxes (or pumping rates) may have partially compensated.

In this work, conductivity is parameterized as piecewise constant corresponding to mapped (deterministic) hydrofacies. Our ongoing research has relaxed this assumption by (1) highly parameterized inversion where conductivity is estimated for each grid cell (more flow measurements are needed to condition this inversion); (2) describing conductivity as piecewise functions to better capture sub-hydrofacies heterogeneity as well as abrupt facies changes (no additional flow measurements needed); (3) facies boundaries are estimated along with the parameters, source/sink terms, and flow field. Although this study does not address uncertainty in inversion due to the uncertain hydrofacies distribution, the inverse method can be easily combined with facies modeling to quantify parameter and flow field uncertainty (Wang et al. 2013). Inversion is currently conditioned by hydrodynamic data; future work will extend the technique to allow joint inversion with indirect measurements by developing appropriate regularization constraints.

Because the new method is developed with the Dupuit-Forchheimer assumption, it is applicable only to problems where horizontal flow dominates for which all wells are fully penetrating. Caution is needed when applying the method to problems where vertical flow is significant for which three-dimensional techniques will likely be needed. Because the pump test solution in the approximating functions is based on the Thiem equation, near-wellbore effects (e.g., wellbore storage, partial penetration, and skin effects) cannot be accounted for. Areal recharge or leakage is not considered, which can potentially be addressed by superposing additional recharge terms to the approximating functions (Zhang 2014). The key to developing the physically based method to address more complex problems is to find appropriate approximating functions to describe the local flow field.

Conclusion

A physically based inverse method is developed to simultaneously estimate conductivity tensors (K) and flow field for a confined aquifer under ambient flow or pumping condition. To represent pumping and injection using a coarse inversion grid, hybrid formulations are used in the approximating functions, while coordinate transform technique is employed to obtain tensor conductivities. Unlike indirect inverse techniques, the new method does not require forward flow simulations to assess data-model misfits; thus knowledge of aquifer BC is not needed. The method directly incorporates noisy observations (i.e., hydraulic heads, Darcy fluxes, or well rates) at the measurement locations, without solving a boundary value problem. Given sufficient measurements, it yields well-posed systems of equations that can be solved efficiently

with nonlinear optimization. The method is successfully tested on aquifer problems with regular and irregular geometries, different hydrofacies and flow patterns, and increasing conductivity anisotropy ratios. Key results are summarized as follows:

- All problems yield stable inverse solutions under increasing measurement errors.
- For a given quantity and quality of the observations, inversion accuracy is most affected by the conductivity anisotropy ratio (K_y/K_x).
- Accuracy in estimating K is also affected by the flow pattern: within a hydrofacies, when a Darcy flux component is very small, the corresponding directional conductivity perpendicular to flow becomes less identifiable.
- Inversion is successful if the location of aquifer boundaries is unknown. Compared to indirect techniques which often require the forward model to extend to some physical boundaries, problem domain for the new inversion can be defined by the measurement location. Therefore, we do not need to seek out physical boundaries with the desired BC characteristics which may lie far from the area of interest.
- In ambient flow, in addition to water levels, subsurface flux (or flow rate) measurements are needed for the inversion to succeed; under pumping condition, pumping rates are needed while flux measurements are not. With aquifer stimulation, data requirement of the method is not much greater than that of interpreting well tests.

Acknowledgments

This work was supported by the University of Wyoming Center for Fundamentals of Subsurface Flow of the School of Energy Resources (Grant Number: WYDEQ49811ZHNG). The authors acknowledge helpful comments from three anonymous reviewers and the editor-in-chief.

References

Chin, D.A. 2006. *Water Resources Engineering*, 2nd ed. Upper Saddle River, New Jersey: Prentice Hall.

Coleman, T.F., and Y. Li. 1996. An interior, trust region approach for nonlinear minimization subject to bounds. *SIAM Journal on Optimization* 6: 418–445.

Davis, S.N., G.M. Thompson, H.W. Bentley, and G. Stiles. 1980. Ground-water tracers – A short review. *Groundwater* 18, no. 1: 14–23.

Doherty J. 2005. PEST. http://www.pesthomepage.org/Home.php (accessed March 15, 2013).

Domzalski, S., J.J. Pop, W.G. Boydell, and A. Hadbi. 2003. Multilayer modelling to define a fluvial sandstone confined aquifer's dynamic structure using multistation multiprobe formation tester measurements. Paper SPE 84094, presented at the SPE Annual Technical Conference and Exhibition, Denver, CO, October 5–8.

Grisak, G., W.F. Merritt, and D.W. Williams. 1977. A fluoride borehole dilution apparatus for groundwater velocity measurements. *Canadian Geotechnical Journal* 14: 554–561.

Labaky, W., J.F. Devlin, and R.W. Gillham. 2009. Field comparison of the point velocity probe with other groundwater velocity measurement method. *Water Resources Research* 45: W00D30. DOI:10.1029/2008WR007066.

Gellasch, C., K. Bradbury, D. Hart, and J. Bahr. 2013. Characterization of fracture connectivity in a siliciclastic bedrock aquifer near a public supply well (Wisconsin, USA). *Hydrogeology Journal* 21, no. 2: 383–399.

Harbaugh, A.W., E.R. Banta, M.C. Hill, and M.G. McDonald. 2000. MODFLOW-2000, the U.S. Geological Survey modular ground-water model–User guide to modularization concepts and the Ground-Water Flow Process: U.S. Geological Survey Open File Report 00-92, 121. Reston, Virginia: USGS.

Hill, M.C., and C.R. Tiedeman. 2007. *Effective Groundwater Model Calibration: With Analysis of Data, Sensitivities, Predictions, and Uncertainty*, 1st ed. Hoboken, New Jersey: John Wiley & Sons, Inc.

Hunt, R., M. Anderson, and V.A. Kelson. 1998. Improving a complex finite-difference ground water flow modeling through the use of an analytical element screening model. *Groundwater* 36: 1011–1017.

Irsa, J., and Y. Zhang. 2012. A new direct method of parameter estimation for steady state flow in heterogeneous aquifers with unknown boundary conditions. *Water Resources Research* 48: W09526. DOI:10.1029/2011WR011756.

Jiao, J.Y., and Y. Zhang. 2014. Two-dimensional inversion of confined and unconfined aquifers under unknown boundary conditions. *Advances in Water Resources* 65: 43–57.

Molz, F.J., G.K. Boman, S.C. Young, and W.R. Waldrop. 1994. Borehole flowmeters: Field application and data analysis. *Journal of Hydrology* 163: 347–371.

Moore, C., and J. Doherty. 2006. The cost of uniqueness in groundwater model calibration. *Advances in Water Resources* 29: 605–623.

Moré, J.J. 1977. The Levenberg-Marquardt algorithm: Implementation and theory. In *Numerical Analysis*. Lecture Notes in Mathematics, Vol. 630, ed. G.A. Watson, 105–116.

Neuman S.P., A. Blattstein, M. Riva, D.M. Tartakovsky, A. Gaudagnini, and T. Ptak. 2007. Type curve interpretation of late-time pumping test data in randomly heterogeneous aquifers. Water Resources Research 43: W10421. DOI:10.1029/2007WR005871.

Novakowski, K., G. Bickerton, P. Lapcevic, J. Voralek, and N. Ross. 2006. Measurements of groundwater velocity in discrete rock fractures. *Journal of Contaminant Hydrology* 82: 44–60.

Pitrak, M., S. Mares, and M. Kobr. 2007. A simple borehole dilution technique in measuring horizontal ground water flow. *Groundwater* 45, no. 1: 89–92.

Post, V.E.A., and J.R. von Asmuth. 2013. Review: Hydraulic head measurements—New technologies, classic pitfalls. *Hydrogeology Journal* 21, no. 4: 737–750.

Ptak, T., M. Piepenbrink, and E. Martac. 2004. Tracer tests for the investigation of heterogeneous porous media and stochastic modelling of flow and transport—A review of some recent developments. *Journal of Hydrology* 294: 122–163.

Rojas, R., L. Feyen, and A. Dassargues. 2008. Conceptual model uncertainty in groundwater modeling: Combining generalized likelihood uncertainty estimation and Bayesian model averaging. *Water Resources Research* 44: W12418. DOI:10.1029/2008WR006908.

The Mathworks. 2012. Optimization toolbox for use with MATLAB, User's Guide, Version 2. www.mathworks.com/help/release/R13sp2/pdf-doc/optim/optim_tb.pdf (accessed January 2014).

Wang, D., Y. Zhang, and J. Irsa. 2013. Dynamic data integration and stochastic inversion of a two-dimensional confined aquifer. In Proceeding of the 2013 AGU Hydrology Days.

http://hydrologydays.colostate.edu/Papers_13/Dongdong_paper.pdf (assessed August 1, 2014).

Zhang, Y. 2014. Nonlinear inversion of an unconfined aquifer: Simultaneous estimation of heterogeneous hydraulic conductivities, recharge rates, and boundary conditions. *Transport in Porous Media*. DOI: 10.1007/s11242-014-0275-x.

Zhang, Y., J. Irsa, and J.Y. Jiao. 2014. Three-dimensional aquifer inversion under unknown boundary conditions. *Journal of Hydrology* 509: 416–429.

Zhang, Y., C.W. Gable, and M. Person. 2006. Equivalent hydraulic conductivity of an experimental stratigraphy-Implications for basin-scale flow simulations. *Water Resources Research* 42: W05404. DOI:10.1029/2005WR004720.

Zhou, H., J.J. Gomez-Hernandez, and L. Li. 2014. Inverse methods in hydrogeology: Evolution and recent trends. *Advances in Water Resources* 63: 22–37.